Progress In Electromagnetics Research, PIER 12, 251–275, 1996

FINITE DIFFERENCE TIME DOMAIN CHARACTERIZATION OF INDOOR RADIO PROPAGATION

L. Talbi and G. Y. Delisle

1. Introduction

In recent years, indoor wireless transmission systems and practical applications of radio LAN have become a very active area of research. Most of the research efforts were oriented toward the statistical characterization of the signal or the generalization of ray tracing techniques to deal with complex situations which arise in an indoor environment[1–3]. The propagation behavior in any in-building environment is a difficult to predict phenomenon which depends notably on the building structure and the operating frequency. The presence of

many obstacles and scatterers leads to multipath signals and shadow fading, therefore limiting the performance of communication systems by reducing the coverage region of the signal. On the other hand, dispersion due to delay spread limits the maximum data rate that can be achieved in a wireless indoor channel.

The purpose of this paper is to present a novel tool based on a numerical technique which can be used to model the indoor radio channel. By converting Maxwell's time-dependent equations into difference equations with respect to specific field positions on an elementary lattice, the FDTD technique provides a simple and effective technique for the modeling of a field distribution inside a room. The system is then solved in a time marching sequence by alternately calculating the electric and magnetic fields in an interlaced spatial grid cell. Given the location of an electromagnetic source and a complete description of the environment in terms of its dielectric parameters (permittivity (ε), permeability (μ), conductivity (σ)), this method provides the ability to assess the electric and magnetic fields [4,5]. Hence, it can predict limitation due to coverage region and bit rate limit by evaluating the steady-state propagation and the channel impulse response respectively.

The FDTD technique is a relatively mature technique even though significant research efforts are directed toward the extension of its capabilities. The advent of powerful computers which have the capacity to manipulate and store large blocks of spatial information makes it competitive with more classical techniques such as the Finite Element Method (FEM). The FDTD method was first introduced by Yee in 1966 [6] and it has two distinct advantages over previously used approaches. First, and most important, it is simple to implement, no matter how complex the structures or mediums are, as long as the electric parameters of the structures (ε and σ) can be assigned to each lattice point. Second, the required memory and execution time increase only linearly with N, the total number of field components.

This paper starts with a brief introduction of basic equations in section II. Following this, section III gives a quick review of the FDTD algorithm and section IV deals with the simulation of the antenna source using the equivalence principle. Sections V and VI deal with the final FDTD implementation to solve the proposed problem while

section VII pertains to experimental and numerical results obtained in different sites for narrow and wideband cases aiming to validate our technique. It also illustrates the possibilities of adequate post-processing of the Time-Domain data to visualize the history of electromagnetic transient phenomenon. The last section deals with the conclusion.

2. Application of FDTD Algorithm to Wave Propagation

Electromagnetic field phenomenon prediction on a macroscopic state is governed by Maxwell's equations, where the electric and magnetic intensities $\vec{E}$ and $\vec{H}$ are related to the electric and magnetic flux densities $\vec{D}$ and $\vec{B}$ and the current density $\vec{J}$, namely:

$$\nabla \times \vec{E} = -\frac{\partial \vec{B}}{\partial t} \tag{1}$$

$$\nabla \times \vec{H} = \frac{\partial \vec{D}}{\partial t} + \vec{J} \tag{2}$$

$$\nabla \cdot \vec{D} = \rho \tag{3}$$

$$\nabla \cdot \vec{B} = 0 \tag{4}$$

Using the constitutive equations which relate the field to the properties of the medium, given by:

$$\vec{D} = \varepsilon \vec{E} \tag{5}$$

$$\vec{B} = \mu \vec{H} \tag{6}$$

$$\vec{J} = \sigma \vec{E} \tag{7}$$

and for an isotropic medium with no charges (ρ =0), the equations (1) and (2) relative to a free source point, are expressed in a rectangular coordinate system (x,y,z) as:

$$\left.\begin{aligned}\frac{\partial H_x}{\partial t} &= \frac{1}{\mu}\left[\frac{\partial E_y}{\partial z} - \frac{\partial E_z}{\partial y}\right]\\ \frac{\partial H_y}{\partial t} &= \frac{1}{\mu}\left[\frac{\partial E_z}{\partial x} - \frac{\partial E_x}{\partial z}\right]\\ \frac{\partial H_z}{\partial t} &= \frac{1}{\mu}\left[\frac{\partial E_x}{\partial y} - \frac{\partial E_y}{\partial x}\right]\end{aligned}\right\} \tag{8}$$

$$\left.\begin{aligned}\frac{\partial E_x}{\partial t} &= \frac{1}{\varepsilon}\left[\frac{\partial H_z}{\partial y} - \frac{\partial H_y}{\partial z} - \sigma E_x\right]\\ \frac{\partial E_y}{\partial t} &= \frac{1}{\varepsilon}\left[\frac{\partial H_x}{\partial z} - \frac{\partial H_z}{\partial x} - \sigma E_y\right]\\ \frac{\partial E_z}{\partial t} &= \frac{1}{\varepsilon}\left[\frac{\partial H_y}{\partial x} - \frac{\partial H_x}{\partial y} - \sigma E_z\right]\end{aligned}\right\} \tag{9}$$

Note that $\varepsilon = \varepsilon_r\varepsilon_0$ and $\mu = \mu_r\mu_0$, and for free space $(\varepsilon_r = 1, \mu_r = 1, \sigma = 0)\varepsilon_0 = 8.854 \times 10^{-12} F/m$ and $\mu_0 = 4\pi \times 10^{-7} H/m$.

To solve the system of Maxwell's equations numerically, Yee[6] has proposed an approach which divides the medium of interest into a mesh of lattices. $\delta x, \delta y,$ and δz are the dimensions of unit lattice. A space lattice point (*i,j,k*) is then denoted as:

$$(i, j, k) = (i\delta x, j\delta y, k\delta z) \tag{10}$$

Any function of space and time is evaluated as:

$$F^n(i, j, k) = F(i\delta x, j\delta y, k\delta z, n\delta t) \tag{11}$$

and its space and time partial derivatives are set up to central-difference approximations as:

$$\frac{\partial F^n(i, j, k)}{\partial x} = \frac{F^n(i, j, k) - F^n(i-1, j, k)}{\delta x} + \text{order } (\delta x^2) \tag{12}$$

$$\frac{\partial F^n(i, j, k)}{\partial t} = \frac{F^{n+\frac{1}{2}}(i, j, k) - F^{n-\frac{1}{2}}(i, j, k)}{\delta t} + \text{order } (\delta t^2) \tag{13}$$

where δt is the time discretization interval. Yee positioned the components of $\vec{E}$ and $\vec{H}$ at half-step intervals around a unit cell (Fig. 1). The $\vec{E}$ and $\vec{H}$ fields are evaluated at alternate half-time steps, giving effectively central-difference expressions for both the space and time derivatives. So, if the components of $\vec{E}$ are calculated at $n\delta t$, where n is any non-negative integer, the components of H are then calculated at $(n+\frac{1}{2})\delta t$.

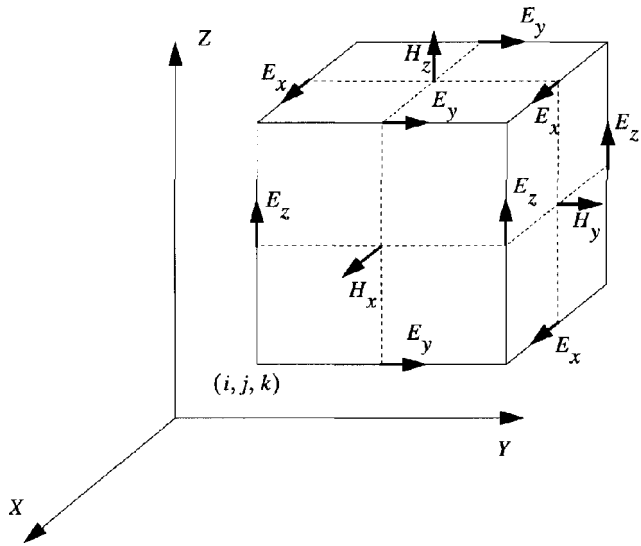

Figure 1. A unit lattice cell.

Applying the above rules, the system (Eqs. 8–9) provides finite-difference time-stepping expressions for electric and magnetic field components. The results obtained are shown in Table 1. As noted earlier, all quantities on the right-hand side of each time-stepping expression are known (stored in computer memory), so that the expressions are fully explicit and well suited for parallel or vector-array-processing computers.

$\vec{H}$ Components

$$H_x^{n+\frac{1}{2}}(i,j,k) = H_x^{n-\frac{1}{2}}(i,j,k) + HM_y[\,E_z^n(i,j-1,k) - E_z^n(i,j,k)\,] + HM_z[\,E_y^n(i,j,k) - E_y^n(i,j,k-1)\,]$$

$$H_y^{n+\frac{1}{2}}(i,j,k) = H_y^{n-\frac{1}{2}}(i,j,k) + HM_x[\,E_z^n(i,j,k) - E_z^n(i-1,j,k)\,] + HM_z[\,E_x^n(i,j,k-1) - E_x^n(i,j,k)\,]$$

$$H_z^{n+\frac{1}{2}}(i,j,k) = H_z^{n-\frac{1}{2}}(i,j,k) + HM_y[\,E_x^n(i,j,k) - E_x^n(i,j-1,k)\,] + HM_x[\,E_y^n(i-1,j,k) - E_y^n(i,j,k)\,]$$

$\vec{E}$ Components

$$E_x^{n+1}(i,j,k) = TM(i,j,k)E_x^n(i,j,k) + EM_y(i,j,k)\left[H_z^{n+\frac{1}{2}}(i,j+1,k) - H_z^{n+\frac{1}{2}}(i,j,k)\right] + EM_{Zz}(i,j,k)\left[H_y^{n+\frac{1}{2}}(i,j,k) - H_y^{n+\frac{1}{2}}(i,j,k+1)\right]$$

$$E_y^{n+1}(i,j,k) = TM(i,j,k)E_y^n(i,j,k) + EM_z(i,j,k)\left[H_x^{n+\frac{1}{2}}(i,j,k+1) - H_x^{n+\frac{1}{2}}(i,j,k)\right] + EM_x(i,j,k)\left[H_z^{n+\frac{1}{2}}(i,j,k) - H_z^{n+\frac{1}{2}}(i+1,j,k)\right]$$

$$E_z^{n+1}(i,j,k) = TM(i,j,k)E_z^n(i,j,k) + EM_x(i,j,k)\left[H_y^{n+\frac{1}{2}}(i+1,j,k) - H_y^{n+\frac{1}{2}}(i,j,k)\right] + EM_y(i,j,k)\left[H_x^{n+\frac{1}{2}}(i,j,k) - H_x^{n+\frac{1}{2}}(i,j+1,k)\right]$$

Medium Constants ($l = x, y, z$)

$$HM_l = \frac{\delta t}{\mu_0}\cdot\frac{1}{\delta l} \qquad TM(i,j,k) = \frac{1-\dfrac{\delta t\cdot\sigma(i,j,k)}{2\varepsilon_0\varepsilon_r(i,j,k)}}{1+\dfrac{\delta t\cdot\sigma(i,j,k)}{2\varepsilon_0\varepsilon_r(i,j,k)}} \qquad EM_l(i,j,k) = \frac{\dfrac{\delta t}{\varepsilon_0\varepsilon_r(i,j,k)}}{1+\dfrac{\delta t\cdot\sigma(i,j,k)}{2\varepsilon_0\varepsilon_r(i,j,k)}}\cdot\frac{1}{\delta l}$$

Table 1. Maxwell's curl equations in finite-difference scheme.

3. Simulation of the Source

In the previous discussions, relations existing among the electromagnetic field vectors have been studied, but so far no consideration

has been given to the means how to deal with the source from where the field is emerged. This can be done with the equivalence principle.

As it is shown [7], two sources producing the same field within a region of space are said to be equivalent within that region. Assuming that the source is inside a volume Ω, the field outside Ω can be found using the equivalence principle approach: Let the field inside Ω be zero; it causes a discontinuity on Σ surface of Ω. To satisfy the boundary conditions, the tangential fields $\hat{n} \times \vec{H}$ and $\vec{E} \times \hat{n}$ are specified on Σ, where $\hat{n}$ is the unit normal vector of Σ. In so doing, the real source inside Ω is replaced by secondary sources or fictitious sources. It is easy to understand that $\hat{n} \times \vec{H} = \vec{J}_e^s$ is the electric current density and $\vec{E} \times \hat{n} = \vec{J}_m^s$ is magnetic current density.

A given distribution of electric and magnetic fields on a closed surface drawn about the antenna structure can be cancelled by placing a suitable distribution of electric and magnetic current sheets $(\vec{J}_e^s, \vec{J}_m^s)$ flowing on the closed surface [7,8] according to Huygen's principle. Hence the radiation computed from the electric and magnetic current sheets is identical to the radiation which might be produced by the original source inside the closed surface.

Knowing the radiation pattern G (θ, ϕ) of the source antenna in far-field condition, the real source is replaced by an artificial surface Σ with fictitious sources lying on Σ. The minimum distance between this surface and the original source is given by the far-field condition which relates the wavelength λ to the maximum dimension of the source antenna D_{ant}. All the above considerations are summarized in Fig. 2.

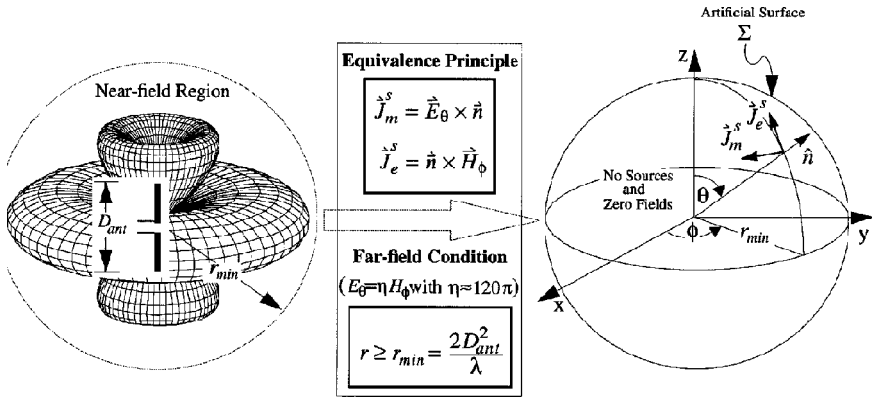

Figure 2. Equivalence principle with far-field condition.

Implementation of the Equivalence Principle

Maxwell's curl equations, applied to the approximate surface grid points which involve the fictitious sources have the following form:

$$\nabla \times \vec{E} = -\mu_0 \frac{\partial \vec{H}}{\partial t} - \vec{J}_m \tag{14}$$

$$\nabla \times \vec{H} = \varepsilon_0 \frac{\partial \vec{E}}{\partial t} + \vec{J} \tag{15}$$

with $\vec{J} = \vec{J}_d + \vec{J}_e$ and $\vec{J}_d = \sigma \vec{E}$ is the conduction current density. To implement the equivalence principle into a finite difference computer program, a surface Σ having the form of a spheroid box is considered with radius respecting the far-field condition and enclosing the source. By a suitable conversion from spherical coordinates (r_{min}, θ, ϕ) to cartesian ones (i_s, j_s, k_s) , the fictitious sources are given as follows:

$$\begin{bmatrix} j_{0,mx} \\ j_{0,my} \\ j_{0,mz} \end{bmatrix} = \frac{E_\theta(\theta,\phi)}{\Delta l} \begin{bmatrix} -\sin\phi \\ \cos\phi \\ 0 \end{bmatrix} \tag{16}$$

$$\begin{bmatrix} j_{0,ex} \\ j_{0,ey} \\ j_{0,ez} \end{bmatrix} = \frac{H_\theta(\theta,\phi)}{\Delta l} \begin{bmatrix} -\cos\theta\cos\phi \\ -\cos\theta\sin\phi \\ \sin\theta \end{bmatrix} \tag{17}$$

Δl is the cell size in the $\hat{n}$ direction. Using Eqs. (3) and (4) the total field on Σ is given by

$$\begin{aligned} H_x^{n+\frac{1}{2}}(i_s,j_s,k_s) = {} & H_x^{n-\frac{1}{2}}(i_s,j_s,k_s) \\ & + HM_z[E_y^n(i_s,j_s,k_s) - E_y^n(i_s,j_s,k_s-1)] \\ & + HM_y[E_z^n(i_s,j_s-1,k_s) - E_z^n(i_s,j_s,k_s)] \\ & + \left(\frac{\delta t}{\mu_0}\right) j_{mx}^n(i_s,j_s,k_s) \end{aligned} \tag{18}$$

$$
\begin{aligned}
&E_x^{n+1}(i_s, j_s, k_s) \\
&= TM(i_s, j_s, k_s) E_x^n(i_s, j_s, k_s) \\
&\quad + EM_y(i_s, j_s, k_s) \left[H_z^{n+\frac{1}{2}}(i_s, j_s + 1, k_s) - H_z^{n+\frac{1}{2}}(i_s, j_s, k_s) \right] \\
&\quad + EM_z(i_s, j_s, k_s) \left[H_y^{n+\frac{1}{2}}(i_s, j_s, k_s) - H_y^{n+\frac{1}{2}}(i_s, j_s, k_s + 1) \right] \\
&\quad - \left(\frac{\delta t}{\varepsilon_0} \right) j_{ex}^{n+\frac{1}{2}}(i_s, j_s, k_s)
\end{aligned} \tag{19}
$$

The other field components are easy to obtain using the same development yielding the corresponding fictitious sources.

4. Implementation of the Algorithm

Before implementing a numerical simulation program, the following modifications which reduce the number of multiplications, additions and the space memory storage requirements are introduced. This way, the algorithm is considerably simplified. This is achieved by defining the constants given in Table 2, where m is an index integer assigned to different materials that constitute the architectural structure. This modification eliminates the need for computer storage of separate $\varepsilon(i, j, k)$ and $\sigma(i, j, k)$ lattices, and it turns out to be a good tool for the implementation of the equivalence principle stated before. One has only to specify the corresponding index to each lattice point to specify the material type.

$m = LATTICE\,(i,j,k)$						
m	$HM_s(m) = \frac{\delta t}{\mu_0}\cdot\frac{1}{\delta s}$	$TM(m) = \frac{1-\frac{\delta t\cdot\sigma(m)}{2\varepsilon_0\varepsilon_r(m)}}{1+\frac{\delta t\cdot\sigma(m)}{2\varepsilon_0\varepsilon_r(m)}}$	$EM_s(m) = \frac{\frac{\delta t}{\varepsilon_0\varepsilon_r(m)}}{1+\frac{\delta t\cdot\sigma(m)}{2\varepsilon_0\varepsilon_r(m)}}\cdot\frac{1}{\delta s}$	$\zeta_{es}(m) = \frac{\delta t}{\varepsilon_0} j_{0,es}(m)$	$\zeta_{ms}(m) = \frac{\delta t}{\mu_0} j_{0,ms}(m)$	*SITUATION*
1	0	0	0	0	0	inside Σ (no sources & no fields)
2	$\neq 0$	$\neq 0$	$\neq 0$	$\neq 0$	$\neq 0$	on Σ (fictitious sources)
0	$\neq 0$	$\neq 0$	$\neq 0$	0	0	free space $\varepsilon_r = 1$ $\sigma = 0$
3 ⋮ N	$\neq 0$	$\neq 0$	$\neq 0$	0	0	N material types $\varepsilon_r > 1$ $\sigma > 0$

Table 2. Medium constants.

$$\begin{aligned} H_x^{n+\frac{1}{2}}(i,j,k) = {} & H_x^{n-\frac{1}{2}}(i,j,k) + HM_z(m)[E_y^n(i,j,k) - E_y^n(i,j,k-1)] \\ & + HM_y(m)[E_z^n(i,j-1,k) - E_z^n(i,j,k)] \\ & + \zeta_{mx}(m)[\alpha(n\delta t)\sin(2\pi f n\delta t)] \end{aligned} \tag{20}$$

$$\begin{aligned} E_x^{n+1}(i,j,k) = {} & TM(m)E_x^n(i,j,k) \\ & + EM_y(m)\left[H_y^{n+\frac{1}{2}}(i,j+1,k) - H_y^{n+\frac{1}{2}}(i,j,k)\right] \\ & + EM_z(m)\left[H_y^{n+\frac{1}{2}}(i,j,k) - H_y^{n+\frac{1}{2}}(i,j,k+1)\right] \\ & - \zeta_{ex}(m)\left[\alpha((n+\frac{1}{2})\delta t)\sin(2\pi f(n+\frac{1}{2})\delta t)\right] \end{aligned} \tag{21}$$

The above equations and the medium constants shown in Table 2 introduce the most compact form of the FDTD algorithm. This algorithm exploits the equivalence principle to simulate the source and avoids loops with IF statements which cause degradation on vectorized compilation of the final program.

Two classes of simulations are of interest: (l) impulse response and (2) CW propagation. For the first case, the transmitting antenna is excited at its center by a gaussian pulse $\alpha(t)$ (Eq. 22) for $t \leq 0$, thus the time-stepping process is going on during a period of predefined time so that all the expected reflections and diffractions reach the observation point. For the latter case, the signal is ideally a pure sinusoid at the carrier frequency, hence $\alpha(t)$ is equal to 1 for all t . The stepping process is terminated when the steady-state is expected after the incident wave has travelled, at least 3 times the longest dimension of the structure. This is done by monitoring peak absolute-values during a period of time corresponding to the last half wave.

$$\alpha(t) = \begin{cases} 1 & \text{Continuous Wave} \\ \alpha_0 \quad e^{-[(t-t_0)/\tau]^2} & \text{Gaussian Pulse} \end{cases} \tag{22}$$

Our algorithm allows us to generate canonical structures such as a cylinder, a rectangular box or a sphere by specifying their principal dimensions and their positions in the global structure. It also allows us to consider more than one source. Figure 3 shows the propagation simulation flowchart based on the FDTD technique. It describes the main stages needed for our purposes.

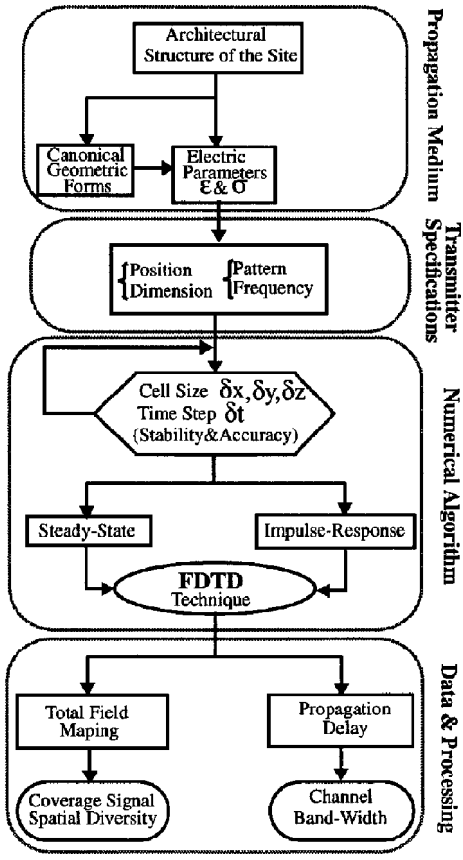

Figure 3. Flow Diagram.

5. Considerations for Algorithm Implementation

A. Accuracy and Stability

The choice of δl and δt is motivated by reasons of accuracy and algorithm stability. To ensure the accuracy of the computed spatial derivatives of the electromagnetic fields, δl must be small compared to a wavelength. $\delta l \leq \lambda/10$ is sufficient to realize less than

7% ($\pm$ 0.6dB) uncertainty [9]. δl should be small enough to permit resolution of geometrical detail forms of the problem considered. The stability condition requires that the numerical errors generated by the time-stepping algorithm do not increase from step to step. The stability criterion first established by Yee has been corrected by Taflove [10], who demonstrated that there is restriction on the choice of δt if δl is selected according to:

$$c \cdot \delta t \leq \frac{1}{\sqrt{\frac{1}{\delta x^2} + \frac{1}{\delta y^2} + \frac{1}{\delta z^2}}} \tag{23}$$

or for a cubic lattice $(\delta l = \delta x = \delta y = \delta z)$

$$c \cdot \delta t \leq \frac{\delta l}{\sqrt{3}} \tag{24}$$

where $\frac{c=1}{\sqrt{\mu_0, \varepsilon_0}}$ is the velocity of propagation in free-space. For whatever signal spectrum, the following additional condition may be useful. In fact, since the FDTD method can be thought of as a "time-sampled" representation of the analog $\vec{E}$ and $\vec{H}$ fields, they must be adequately sampled to ensure the conservation of all information after sampling. Assuming the signal treated by the algorithm is band-limited to $f_{max} H_z$, the minimum sampling rate that does not destroy any information content is $f_{samp} \geq 2 f_{max}$ (Nyquist sampling rate). Thus

$$f_{samp} = \frac{1}{\delta t} \geq 2 f_{max} \tag{25}$$

B. Lattice Truncations

A basic consideration of the FDTD approach to solve electromagnetic field problems is that the outer lattice planes bounding the mesh domain, called the lattice truncation planes, cannot be treated by the algorithm. All these nodes require special treatments. This can be done either by an absorption condition or by assigning linearly increasing values of σ near the lattice boundary. For our purpose, the media in which the total field must be computed are bounded. The presence of reflection and diffraction phenomena make the unrealistic reflections

due to boundary treatment using local absorbing boundary conditions weaker. This is done by extrapolating the fields at the neighboring nodes as $1/r$ where r is the propagation distance(Sommerfeld Condition) [11].

The first order absorbing boundary [12] which costs less in computer storage was chosen. For a mesh of dimension (N_x, N_y, N_z) the outer boundaries are given below. As an example, for the planes $i = 1$ and $i = N_x$, the E_z component is written as:

$$E_z^{n+1}(\mathbf{1}, j, k) = E_z^n(\mathbf{2}, j, k) - \frac{c\delta t - \delta x}{c\delta t + \delta x}\left[E_z^{n+1}(\mathbf{2}, j, k) - E_z^n(\mathbf{1}, j, k)\right] \tag{26}$$

$$E_z^{n+1}(\mathbf{N_x}, j, k) = E_z^n(\mathbf{N_x} - \mathbf{1}, j, k) - \frac{c\delta t - \delta x}{c\delta t + \delta x} \left[E_z^{n+1}(\mathbf{N_x} - \mathbf{1}, j, k) - E_z^n(\mathbf{N_x}, j, k)\right] \tag{27}$$

Knowing all the $\vec{E}$ field components, the remaining $\vec{H}$ components are easily deduced from the algorithm.

Tangential Components	Boundary Planes					
	x		y		z	
E_x			1	N_y	1	N_z
E_y	1	N_x			1	N_z
E_z	1	N_x	1	N_y		

Table 3. Boundary Planes for (N_x, N_y, N_z) Mesh.

C. Electrical Properties of Materials

There is a lack of knowledge of dielectric properties of common building materials at UHF band. Those which are available are limited to some homogeneous materials and at a specified frequency. Usually

in buildings, composite materials are employed and these include mixtures of dielectric and conductive materials which behave as lossy dielectric. Composite materials which have a conductivity as well as complex permittivity $(\hat{\varepsilon} = \varepsilon' - j\varepsilon'')$ are described by considering an equivalent conductivity that includes the dielectric's loss factor. A chart displaying the relative permittivity and loss tangent $(tan\delta = \varepsilon''/\varepsilon')$ of principal classes of solid materials useful in modeling is given by [13].

6. Simulation and Experimental Results

Two kinds of measurements have been carried out; narrow-band measurements and path loss as a function of distance. They were performed at a frequency of 893 MHz using a Rx-900 UHF receiver (Comlab inc.) with a bandwidth of approximately 5 MHz. The transmitter is kept at a fixed location while the receiver, mounted on automatic tracking and drive system cart, guided by a wire determining the path, placed on the floor, moves at approximately 5 cm/s along a predetermined path. An optical encoder, fixed to an independent wheel on the cart is used to sample the received signal every 0.5 mm [14,15].

Wideband measurements, radar-like impulse response, were performed at a frequency of 918 MHz modulated by a train of 5 ns pulses with 3.4 μs repetition period, with receiving bandwidth of 1 GHz. Both antennas are vertically polarized and have radiation patterns which are omnidirectional in the horizontal plane with 3 dB gain each. Measurement results are obtained for a fixed transmitter-receiver location and for all measurements, the antenna height was kept at 1.75m. The details of the apparatus used are given in [15,16] with a simple modifications to cover the appropriate frequency band of interest.

A. Choice of Sites

Due to the limitation on available memory, simulations have been carried out assuming two dimensional problems, dealing with the vertical polarization (E_z). In this case the z coordinate dependency of the field components is omitted and the FDTD computer program computes E_z, H_x and H_y. In such a case, the Huygen's surface will be a circle instead of a sphere.

The respective measurements have been performed in such a manner that contributions of the ceiling and ground reflections are minimized. Therefore, the transmitter system (fixed station) is located close to the physical center of the room and the heights of the antennas are set at about half the room's height which is close to 3.5 m.

Two typical sites are proposed for setting up measurements and simulations:

1- Site 1: An empty room with effective dimensions including walls 12.18 m $\times$ 4.50 m.

2- Site 2: A complex room which is contiguous to the first room (12.18 m $\times$ 6.21 m). It contains laboratory equipment. Figure 4 shows a sketch of the sites and their main indoor structure.

B. Choice of Program Parameters

The source used in our simulation has the specifications given in Table 4. The antennas are omnidirectional vertical $\lambda/4$ dipoles. The parameters (t_0, τ) given in the same table are used for simulating an impulse response for a transmitted pulse of width about 5 ns. Table 5 gives electric properties used in our simulation. Note that the windows have a metallic mosquito net and the air-conditioning system is coated with dielectric paint.

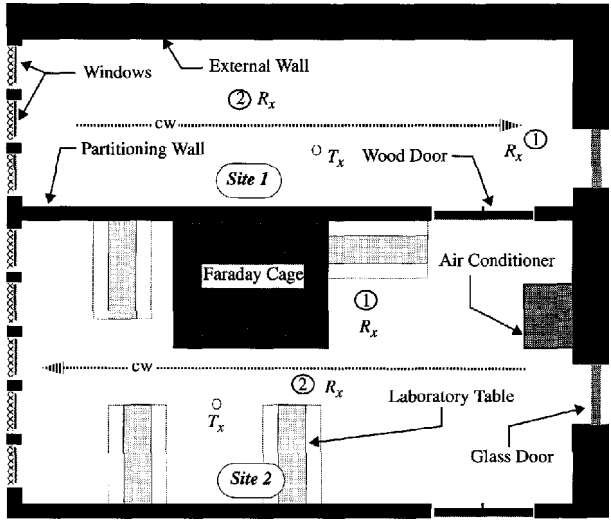

Figure 4. Description of the sites.

The program code is written in C language on a UNIX-based Sun SparcStation ECL. The output data are directly generated using MATLAB code which allows us to perform further signal processing tasks. The execution time requirements of each program are noted in Table 6, considering a high-optimization C compiler used to minimize the execution time of each run.

Impulse Response	*C.W*	Frequency f	893 – 918 MHz	$\lambda\,(mm) \approx 336 - 327$
		Radiation Pattern $G(\theta, \phi)$	$\frac{\cos(k\cos\theta) - \cos k}{\sin\theta}$ 1 (*omnidirectional*)	E-Plan H-Plan $k = \frac{2\pi}{\lambda}$
		Space-Step δl ($\delta x = \delta y = \delta z$)	30 mm	$\delta l \approx \lambda/10$
		Time-Step δt	0.05 ns	$\delta t = \delta l/2c$
	Pulse Parameters	τ	2.5 ns	$t_0 = 2\tau$
		t_0	5 *ns*	
		α_0	1	

Table 4. Summary of the source parameters.

MATERIAL	Concrete-Wall (External-Wall)	Plasterboard-Wall (Partitioning-Wall)	Faraday Cage	Air-Conditioning	Glass of Windows	Wood-Material
m	3	4	5	6	7	8
ε_r	15	14	1	2	8	10
$\sigma\,(S/m)$	10^{-5}	10^{-7}	10^{7}	10^{4}	10^{-2}	0

Table 5. Electrical Properties of Different Materials.

Our best estimate of the execution time that could be required for a 3-dimensional simulations, considering the height for the empty room case, lead to a figure of 8×10^5 s. Therefore an appreciable amount of computer power to make 3-D simulations feasible is required, and the best way to improve this time is provided using parallel or vector-array-processing computers.

	CW		Impulse-Response	
	Time Steps	CPU Time	Time Steps	CPU Time
Empty Room	400 ns	7031.0 s	500 ns	7108.8 s
Complex Site	400 ns	7999.3 s	500 ns	12093.2 s

Table 6. Running-time and corresponding CPU.

C. Discussions

The simulation results pertinent to each site are presented as a mapping of the field after two-dimensional filtering using a Hamming window. Figure 5 shows the mapping obtained for a CW simulation for each site and for transmitter locations as shown in Figure 4. Figure 5a shows that the signal levels on the left (windows) side of the empty room are somewhat greater than those of the right (door) side, although the transmitting antenna is omnidirectional in azimuth. In fact, this is caused by the mettalic mesh structure (mosquito net) of the windows. This kind of data can be useful for the design of personal communication systems and, in fact, one can find the optimal antenna location in a given architectural configuration or search for a suitable spatial diversity. For each simulation result, the path loss field (signal strength) corresponding to a CW measurement scenarios, as shown in Figure 4, are recorded and Figure 6 plots these data for their respective measurements. The simulated and the measured data reveal an interesting and important multipath propagation which depends upon the site and, as it can be seen, reasonable agreement is achieved.

In fact, from a statistical point of view the medians and the variances, for measured and simulated data, are reasonably close. It should be recognized, however, that at this frequency band signals penetrate wall easily and, therefore, contributions from the outside of each room are not negligible. Since the elevation beamwidth of the antennas is close to $70°$, other contributions may also occur from the ceiling and the floor. These contributions maintain a high level for the signal with fewer nulls as shown in our measurement results. All our measurements were conducted without any interfering movement throughout the measurement areas.

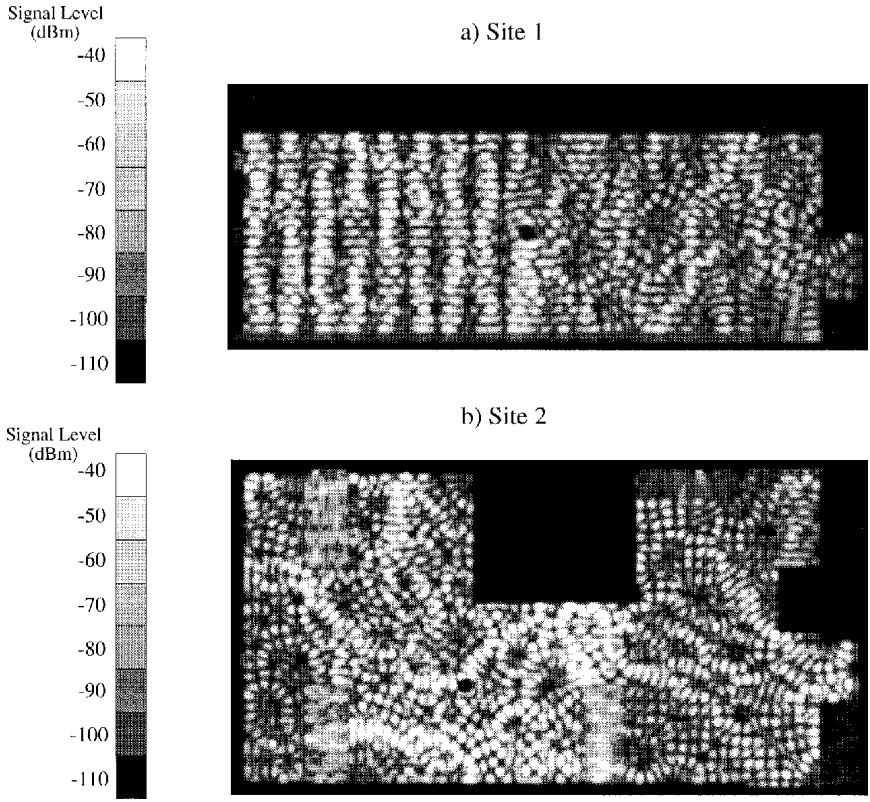

Figure 5. Field mapping in different rooms.

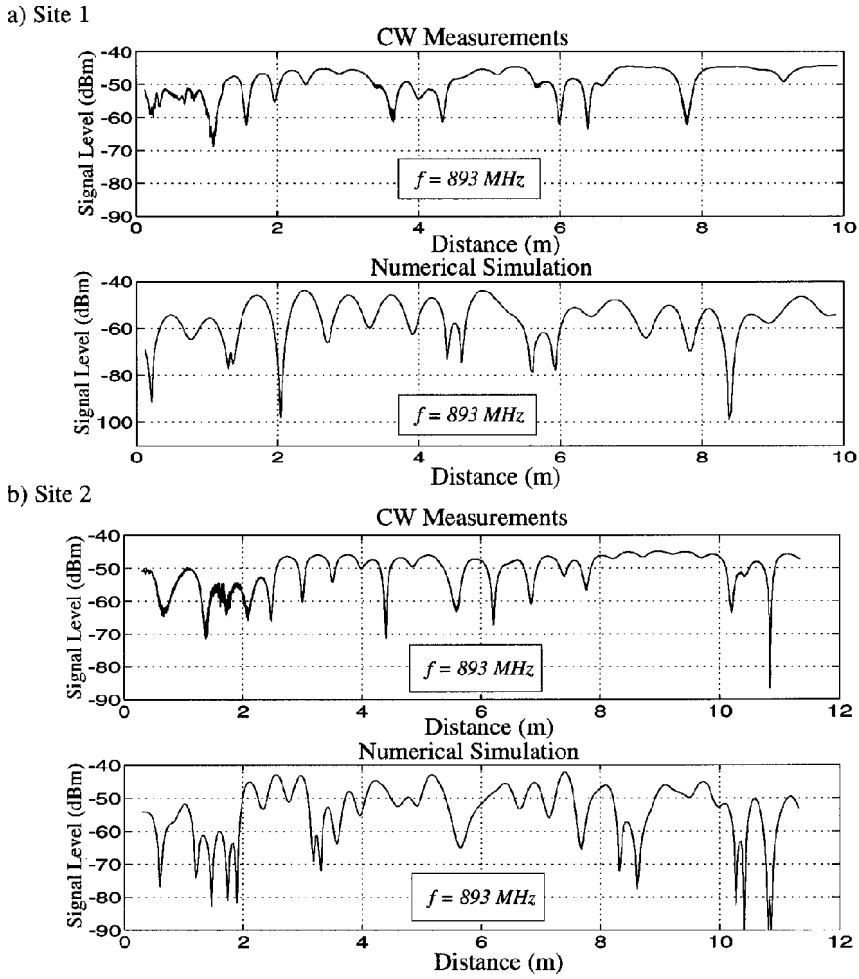

Figure 6. Power signal level vs. distance in different rooms.

For the impulse response simulations, the line-of-sight (LOS) and non line-of-sight (NLOS) scenarios are performed on the complex site by moving the receiver as shown in Figure 4. To allow a good comparison, both numerical and measurements results are normalized to the maximal magnitude of the signal. The results obtained are shown in Figures 7 and 8 for different rooms and different transmitter-receiver locations. For the complex site, Figure 8 shows NLOS and LOS scenarios respectively. There is again an interesting agreement except for

some ripples that appears in our simulations. These can be explained by cancellation of the direct signal with a reflection from the Faraday cage or the fact that the obstacles considered in our 2-dimensions simulation, such as laboratory tables, have heights less than the antenna height. Also the lack of knowledge of the exact dielectric properties of all the materials encountered in these indoor radio communications experiments must affect the results. The energy at 90 ns must be an echo from both ends of the room.

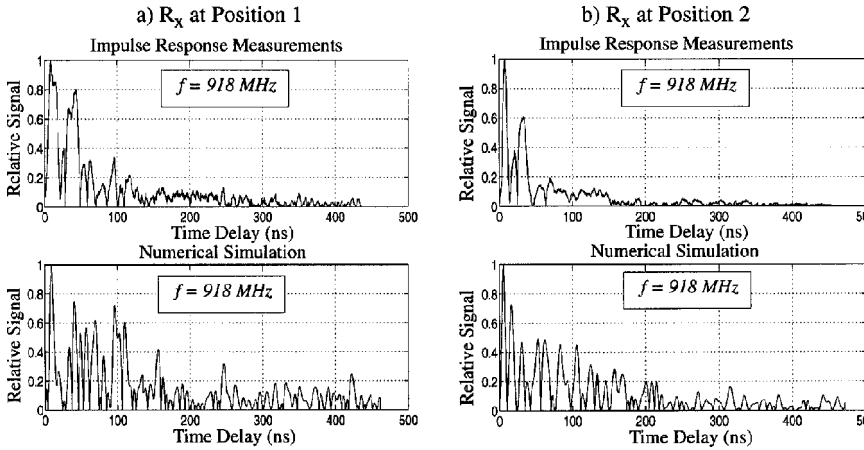

Figure 7. Impulse responses in site 1.

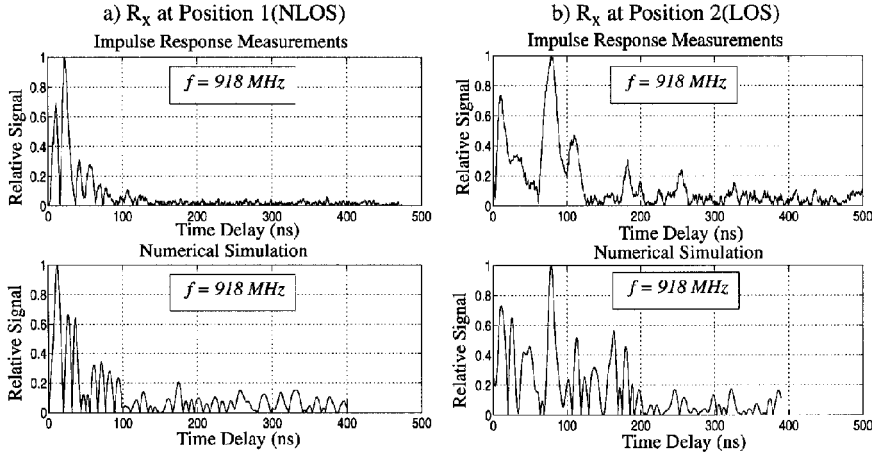

Figure 8. Impulse responses in site 2.

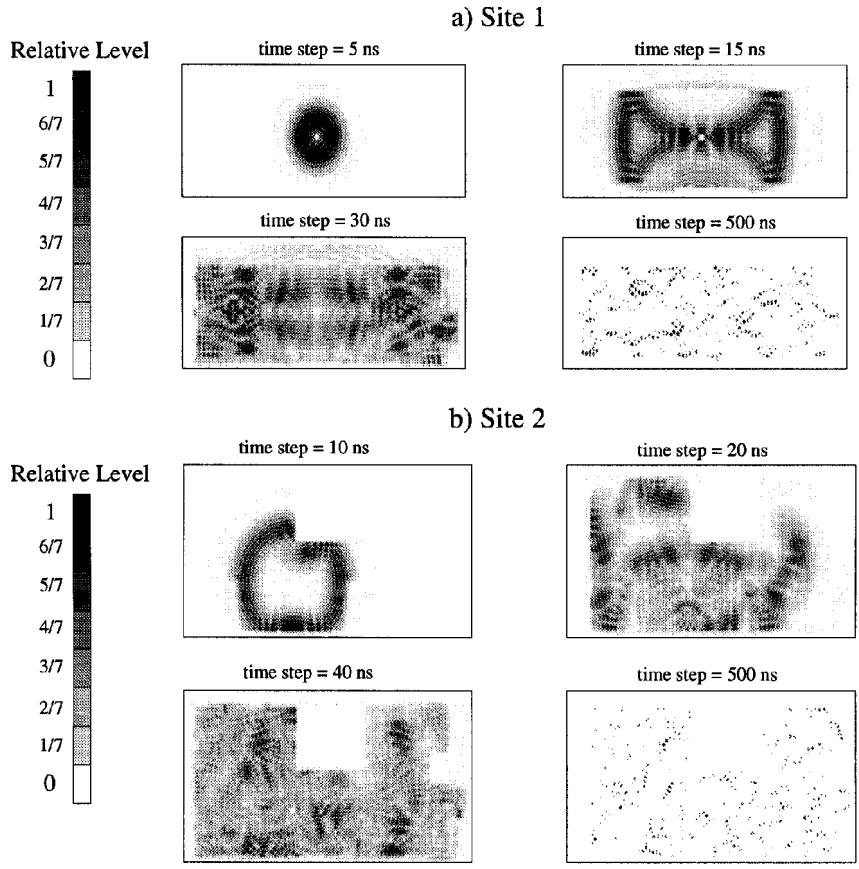

Figure 9. Wave propagation at different steps.

A good understanding of the interaction of electromagnetic waves with complex structures, such as the concept of diffraction, interference and reflection by boundaries, can be obtained by a visualization of propagation history, as explored by looking at the successive snapshots of the time-domain based FDTD technique shown in Figure 9. These two examples of the time domain approach are used to produce computer animation at four different time steps.

7. Conclusion

A numerical method based on FDTD technique has been introduced for the simulation of the indoor radio channel and the radiation pattern of the antennas are incorporated in the global simulation. The validation of the proposed technique has been done with two different media where measurements and simulations results, including wideband and narrowband cases at 918 MHz and 893 MHz respectively, are obtained. A comparison between simulated and experimental results shows a fair agreement for the general behavior of the wave propagation coupled with some discussed details. Results pertaining to the mapping of the signal distributions are presented in order to define the optimal antenna localization to ensure good coverage and the CW results can be used to investigate path loss propagation, statistical distributions of large and small scale fadings. The impulse responses obtained can also be used to assess RMS delay spread, number of reflectors and coherence bandwidth. Thus, the FDTD approach is proven to be viable and a useful means for calculating the parameter keys that characterize the wireless indoor propagation channel.

Acknowledgments

This work has been supported by a grant from the Canadian Institute for Telecommunications Research (CITR), one of the Network of Centers of Excellence of the Government of Canada.

References

1. Saleh, A. A. M., and R. A. Valenzuela, "A statistical model for indoor multipath propagation," *IEEE Journal on Sel. Areas in Comm.* Vol. SAC-S, No. 2, 128–137, Feb. 1987.
2. Rappaport, T.S. "Characterization of UHF multipath indoor radio channels in factory buildings," *IEEE Trans. on Antennas and Propagation,* Vol. 37, 1058-1069, No. 8, Aug. 1989.
3. McKown, J. W., and R. L. Hamilton, "Ray tracing as a design tool for radio networks," *IEEE Network Magazine,* Vol. 5, No. 6, 27–30, Nov. 1991.

4. Talbi, L., and G. Y. Delisle, "Application de la FDTD au Calcul du Champ Électromagnétique à l'Intérieur des Édifices," *Canadian Conference on Electrical and Computer Engineering,* Quebec, Sept. 25–27, 16.5.1–16.5.4, 1991.
5. Lu, Y. E., "Site precise radio wave propagation simulations by time domain finite difference methods," *43rd IEEE Vehicular Technology Conference,* 875–878, 1993.
6. Yee, K. S., "Numerical solution of initial boundary value problems involving Maxwell's equations in isotropic media," *IEEE Trans. Antennas Propagat.,* Vol. AP-14, 302–307, May 1966.
7. Mittra, R., *Computer Techniques for Electromagnetics,* Summa Book, Hemisphere Publishing Corp., New York, 1987.
8. Merewether, D. E., R. Fisher, and F. W. Smith, "On implementing a numeric Huygen's source scheme in a finite difference program to illuminate scattering bodies " *IEEE Trans. on Nuclear Science,* Vol. NS-27, No. 6, 1829–1833, December 1980.
9. Taflove, A., and K. R. Umashankar, "Review of FD-TD Numerical Modeling of Electromagnetic Wave Scattering and Radar Cross Section" *Proc. IEEE,* Vol. 5, May 1989.
10. Taflove, A., and M. E. Brodwin, "Numerical solution of steady-state electromagnetic scattering problems using the time-domaine Maxwell's equations" *IEEE Trans. Microwave Theory Tech.,* Vol. MTT-23, 623–630, August 1975.
11. Sullivan, D. M., D. T. Borup, and O. M. Gandhi, "Use of the finite-difference time-domain in calculating EM absorption in human tissues," *IEEE Trans. Biomedical Eng.,* Vol. BME-34, No. 2,.148–157, Feb. 1987.
12. Mur, G., "Absorbing boundary conditions for the finite-difference approximation for the time-domaine electromagnetic-field equations," *IEEE Trans. Electromagn. Compat.* Vol. EMC-23 , No. 4, 1073–1077, Nov. 1981.
13. Lo, Y. T., and S. W. Lee, *Antenna Handbook,* Van Nostrand Reinhold, Co., New York, 1988.
14. Ahern, J., G.Y. Delisle, and Y. Chalifour, "Indoor Millimeter-Wave Propagation Measurement System," *Canadian Conference on Electrical and Computer Engineering,* Quebec, Sept. 25-27, 9.1.1–9.1.4, 1991.

15. Talbi, L., and G. Y. Delisle, "Measurement results of indoor radio channel at 37.2 GHz," *International Symposium on ANTEM'94,* Ottawa, Ontario, Canada, 9–13, August 1994.
16. Talbi, L., and G. Y. Delisle, "Wideband propagation measurements and modeling at millimeter wave frequencies," *Proc. IEEE-GLOBECOM'94,* San Francisco, California, Vol. 1, 47-51, December 1994.